ELECTRONIC SUPPLEMENTARY INFORMATION

Ion-selective crown ether covalently grafted onto chemically exfoliated MoS_2 as biological fluids sensor

Anastasios Stergiou[a§], Christina Stangel[a§], Ruben Canton-Vitoria[b], Ryo Kitaura[b] and Nikos Tagmatarchis*[a]*

[a] Theoretical and Physical Chemistry Institute, National Hellenic Research Foundation, 48 Vassileos Constantinou Avenue, 11635 Athens, Greece

[b] Department of Chemistry, Nagoya University, Nagoya 464-8602, Japan

[§] Equal contribution

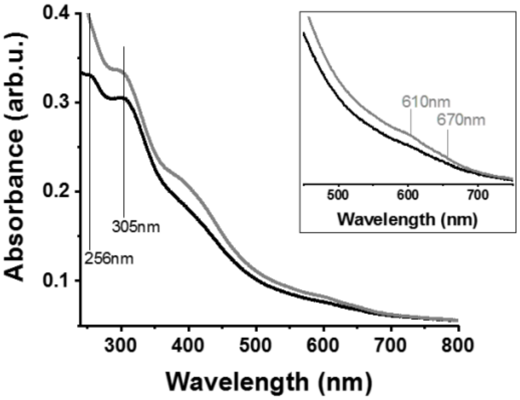

Figure S1. UV-Vis spectra of *ce*-MoS_2 as soon as prepared (black) and after two months stored in the dark (grey), obtained in distilled water. Inset: the region 500-700 nm is presented for clarity.

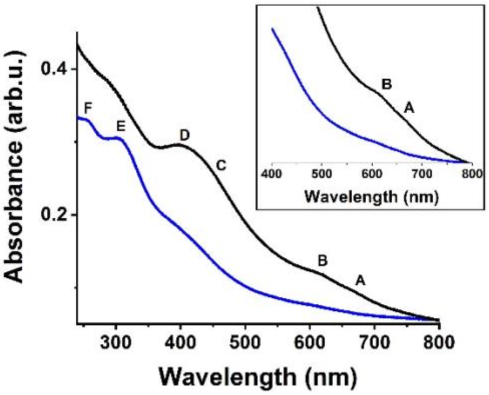

Figure S2. UV-Vis spectra of *ce*-MoS_2 as soon as prepared in alkaline pH (blue) and the recovered nanosheets precipitated in acidic conditions (black), obtained in distilled water.

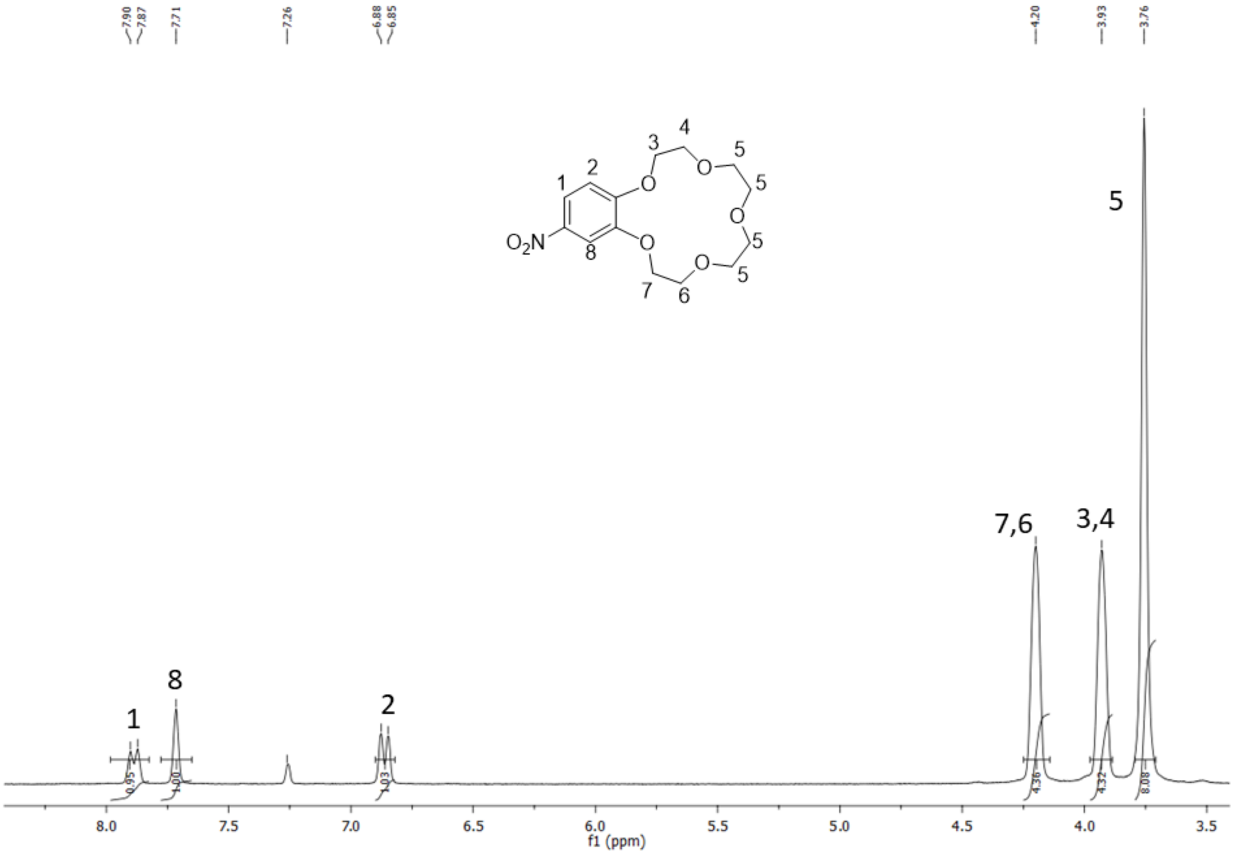

Figure S3. ^{1}H NMR spectrum of 4′-nitrobenzo-15-crown-5 in $CDCl_3$.

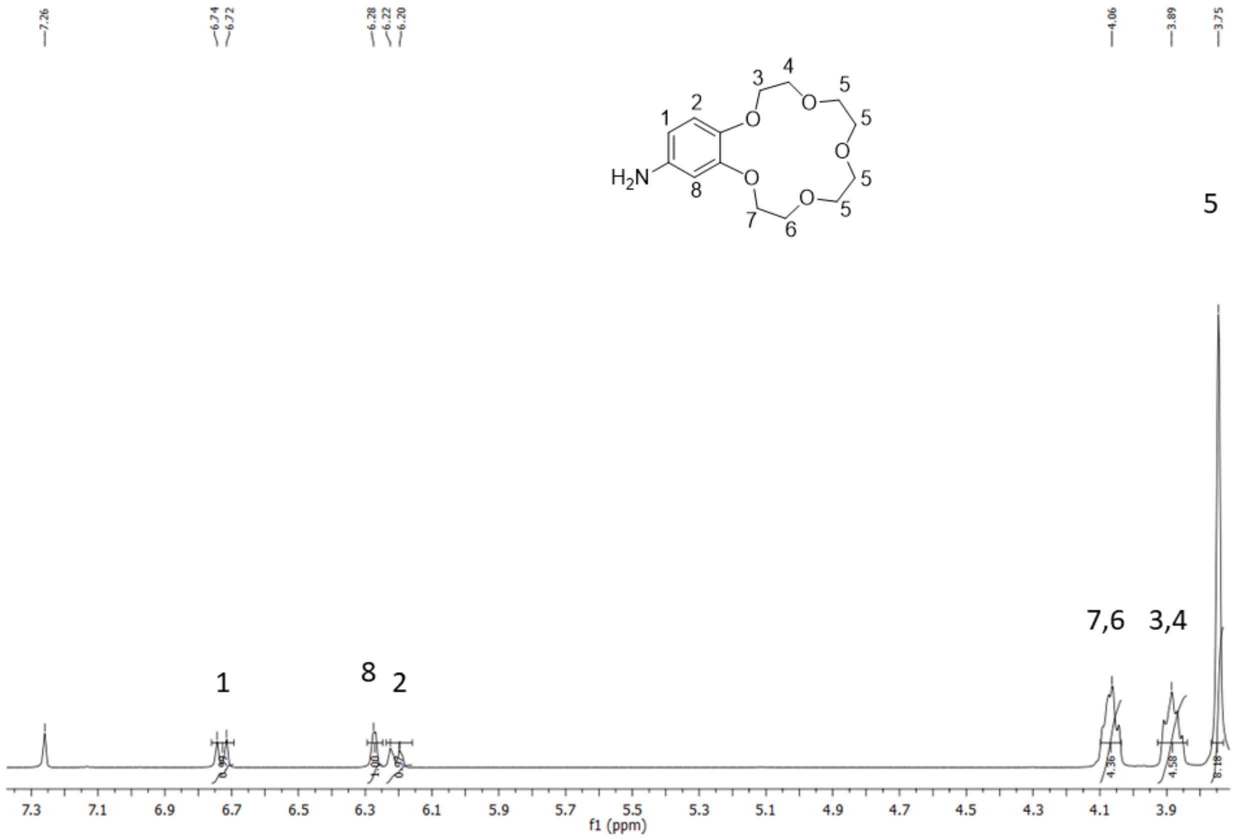

Figure S4. ^{1}H NMR spectrum of 4′-aminobenzo-15-crown-5 in $CDCl_3$.

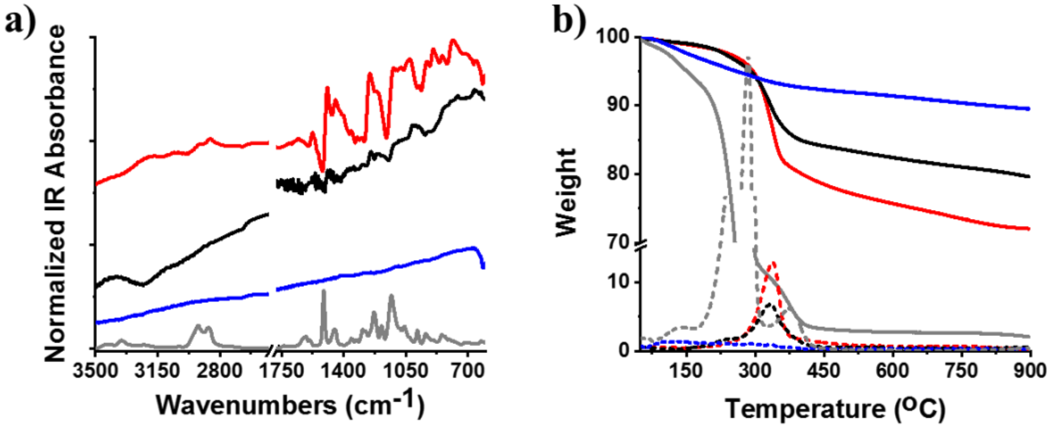

Figure S5. (a) Normalized FT-IR spectra (presented as absorbance) for B15C5 (grey), *ce*-MoS_2 (blue), the reaction towards **B15C5-MoS_2** with excess HCl (black) and stoichiometric HCl (red). (b) TGA curves recorded for B15C5 (grey), *ce*-MoS_2 (blue), the reaction towards **B15C5-MoS_2** with excess HCl (black) and stoichiometric HCl (red), obtained under nitrogen atmosphere. With dashed lines are presented the corresponding curves of the 1st derivative of weight versus temperature.

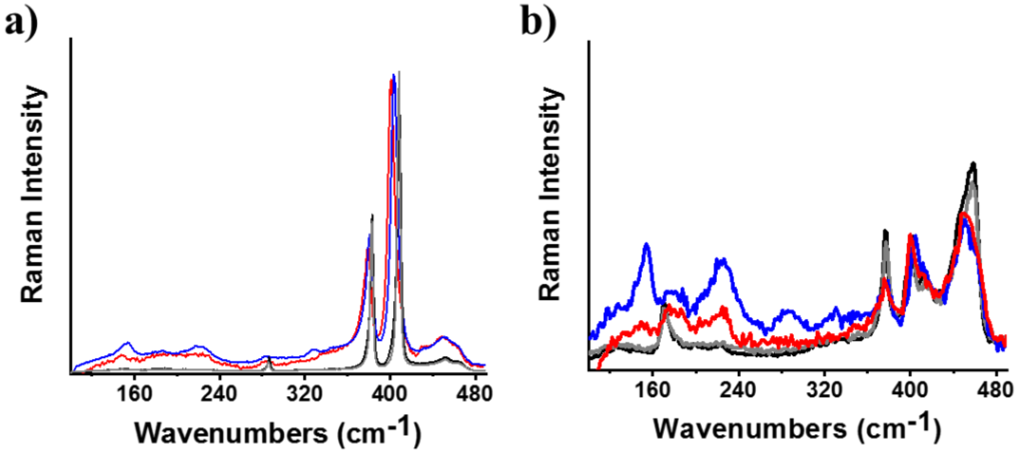

Figure S6. Raman spectra for *ce*-MoS_2 (blue), **B15C5-MoS_2** (red) upon (a) 514 nm excitation, and (b) 633 nm excitation. The spectra of bulk MoS_2 (grey) and exfoliated 2H-MoS_2 (black) are also presented for comparison. All spectra obtained at ambient conditions.

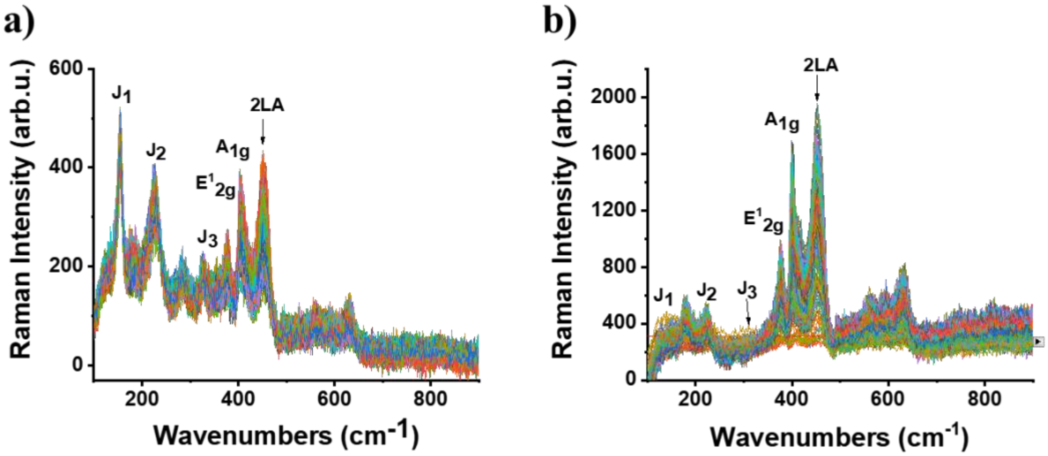

Figure S7. Raman spectra from a 20 μm x 20 μm area (3 nm step, 196 points/spectra) for (a) *ce*-MoS_2 and (b) **B15C5-MoS_2**. Spectra recorded under 633 nm excitation with 0.3 mW/cm^2 power at ambient conditions and used as received for the construction of the Raman maps shown at Figure 3.

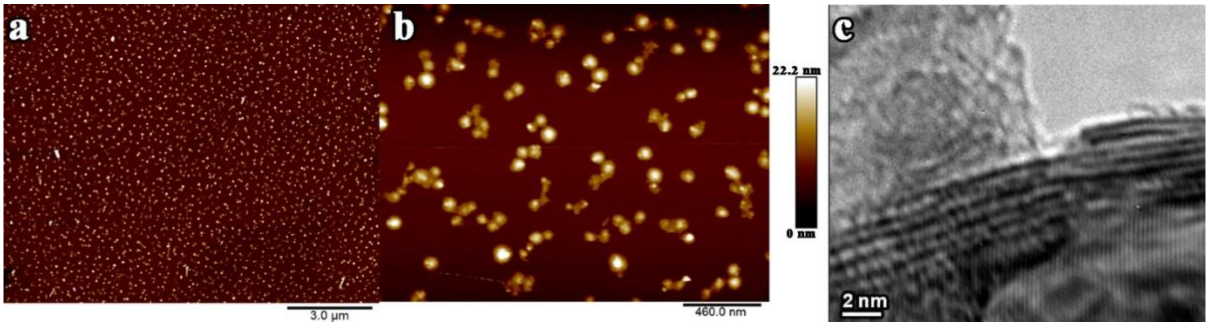

Figure S8. AFM images of *ce*-MoS_2 at (a) low and (b) high magnification. The height scale bar is common in both images. (c) TEM micrograph of *ce*-MoS_2 taken with under focus condition to enhance contrast from MoS_2.

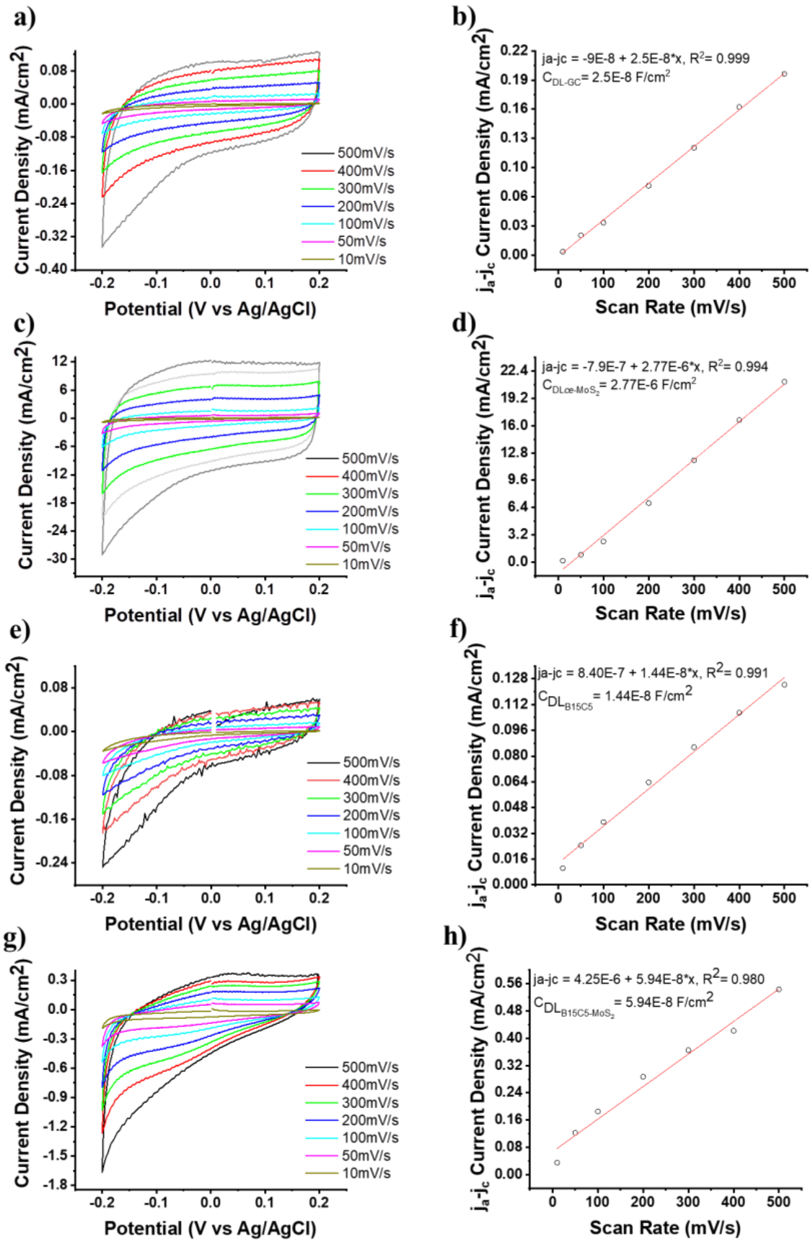

Figure S9. Cyclic voltamographs recorded in nitrogen-saturated 0.5 M H_2SO_4 for (a) glassy carbon (GC) electrode, (c) GC/*ce*-MoS_2, (e) GC/B15C5 and (g) GC/**B15C5-MoS_2** at different scan rates. The corresponding plots of the current density at 0.05 V versus the scan rate are presented in (b), (d), (f), and (h) and used for determining the double layer capacitance of the studied electrodes. All CV data acquired at room temperature, with Ag/AgCl (3.0 M KCl) as reference electrode and a Pt foil as counter electrode.

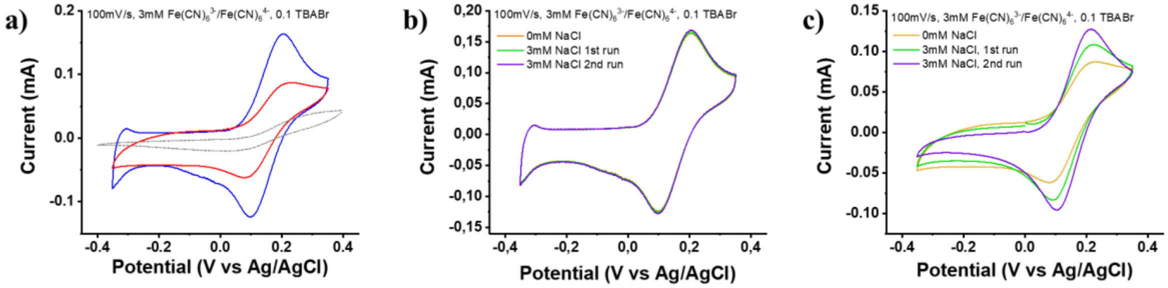

Figure S10. Cyclic voltamographs for (a) GE/B15C5 (grey), GC/*ce*-MoS$_2$ (blue) and GC/**B15C5-MoS$_2$** (red), (b) GC/*ce*-MoS$_2$, and (c) GC/**B15C5-MoS$_2$** at different NaCl concentrations (orange: 0 mM, green: 3 mM 1st CV run out of 2, violet: 3 mM 2nd CV run out of 2. All CVs were recorded in aqueous 0.1 M tetrabutylammonium bromide, in the presence of 3.0 mM K$_4$Fe(CN)$_6$ at room temperature, with Ag/AgCl (3.0 M KCl) as reference electrode and a Pt foil as counter electrode and at a scan rate of 100 mV/s.